CHANDRA DETECTION OF A SYNCHROTRON NEBULA AROUND THE VELA-LIKE PULSAR J1016–5857

F. Camilo, B. M. Gaensler, E. V. Gotthelf, J. P. Halpern, and R. N. Manchester To~appear~in~ApJ

ABSTRACT

We report on a 19ks observation of the pulsar J1016-5857 with the Chandra X-ray Observatory. This "Vela-like" pulsar has rotation period 107 ms, characteristic age 21 kyr, and spin-down power $2.6 \times$ $10^{36} \,\mathrm{ergs}\,\mathrm{s}^{-1}$. A relatively bright centrally peaked source of radius $\approx 25''$ around the radio pulsar position has a spectrum that is well fitted by an absorbed power law with photon index 1.32 ± 0.25 . We regard this as a newly identified pulsar wind nebula that we designate PWN G284.0-1.8. We do not detect the pulsar either as a point X-ray source or as a pulsed source in a 55 ks observation with the Rossi X-ray Timing Explorer (RXTE). The isotropic PWN luminosity is $3 \times 10^{32} \,\mathrm{ergs\,s^{-1}}$ in the 2–10 keV range, for a distance of 3 kpc that is consistent with the measured neutral hydrogen column density. The unpulsed flux from the pulsar is less than 30% of the measured PWN flux. The brightest component of the PWN, near the pulsar, shows extended emission of size $\sim 2''$ that may indicate, by analogy with other young pulsars, the wind termination shock. In the Chandra image we also detect a very faint extended structure $\approx 1' \times 2'$ in size that is highly asymmetric about the pulsar position. This structure is a good match in width and position angle to the tip of a "finger" of radio emission that appears to connect to the nearby supernova remnant G284.3–1.8, but we cannot characterize it further with the available data. There is a variable X-ray point source only 1.5 from the pulsar, which we identify using optical spectroscopy as an accreting binary.

Subject headings: ISM: individual (G284.0–1.8, G284.3–1.8) — pulsars: individual (PSR J1016–5857) — stars: individual (CXOU J101623.6–585542) — supernova remnants

1. INTRODUCTION

Magnetospherically active neutron stars with spin parameters similar to those of the Vela pulsar have proven very useful to study a variety of high-energy processes, such as thermal emission from the surface of young neutron stars, pulsed emission at X-ray energies that can extend to γ -ray energies and potentially power EGRET sources, interaction of the relativistic pulsar wind with the immediate environment as observed through a synchrotron nebula, and interaction of such a pulsar wind nebula (PWN) or the pulsar with any existing supernova remnant (SNR).

PSR J1016-5857 is one of about 25 "Vela-like" pulsars now known, typically having spin periods $P \sim 0.1$ s, characteristic ages $10^4\,\mathrm{yr}\lesssim\tau_c=P/2\dot{P}\lesssim10^5\,\mathrm{yr}$, and spin-down luminosities $\dot{E}=4\pi^2I\dot{P}/P^3\gtrsim10^{36}\,\mathrm{ergs\,s^{-1}}$, where the moment of inertia $I\equiv10^{45}\,\mathrm{g\,cm^2}$. Like half of all Velalike pulsars known, it was discovered in the Parkes multibeam pulsar survey of the Galactic plane (e.g., Manchester et al. 2001). Because pulsars discovered in the multibeam survey are generally farther away than previously known pulsars, they are expected to be fainter and more absorbed sources of X-rays, and for the most part they have yet to be studied with X-ray observatories. PSR J1016-5857 may be particularly interesting because it appeared to be coincident with an Einstein Observatory X-ray source, is positionally coincident with the very tip of a "finger" of radio emission apparently originating from the SNR G284.3-1.8, and is also coincident with an unidentified EGRET source, 3EG J1013–5915, that has characteristics suggesting a possible pulsar origin (Camilo et al. 2001).

For these reasons we obtained short observations with Chandra and RXTE in order to investigate further the nature of the environment of PSR J1016–5857.

2. OBSERVATIONS, ANALYSIS AND RESULTS

2.1. Chandra Observation

PSR J1016–5857 was observed with *Chandra*'s Advanced CCD Imaging Spectrometer (ACIS) on 2003 May 25 (MJD 52784). The pulsar position obtained from radio timing observations (Camilo et al. 2001) was placed on the aim-point of the ACIS S3 CCD. The data were collected in TIMED exposure, VFAINT mode, and the original event files were reprocessed with up-to-date calibration files. All *Chandra* data processing used the latest CIAO tools. There were no periods of abnormally high background, and the effective integration time was 18,615 s.

2.2. RXTE Observation

A 64,450s observation targeting PSR J1016–5857 was obtained by RXTE on 2004 March 6 (MJD 53070). To search for pulsations we analyzed data from the Proportional Counter Array detector (PCA; Jahoda et al. 1996), acquired in the GoodXenon mode. The non-imaging PCA (with a 1° FWHM field of view) is made up of five counter units that are sensitive to X-rays in the 2–60 keV range. During the observation, photon arrival times were collected with better than $100~\mu s$ resolution using a time-weighted average of 3.0 counter units in operation.

2.3. Parkes Timing Observations

PSR J1016–5857 experiences significant "timing noise" that biases its position obtained via timing measurements (Camilo et al. 2001). We have performed fits to three independent Parkes timing data sets, and while the average position is consistent with that of Camilo et al. (2001), which we use here, there is considerable variance, from which we estimate the uncertainty: (J2000.0) R.A. = $10^{\rm h}16^{\rm m}21^{\rm s}.16 \pm 0^{\rm s}.14$, Decl. = $-58^{\circ}57'12''.1 \pm 0''.3$, where the errors should be considered approximate 68%

confidence level estimates. It is possible that future interferometric observations with the Australia Telescope Compact Array will yield a precise pulsar position free of significant systematics.

2

The pulsar has experienced a rotational glitch once since it was discovered (Hobbs et al. 2004). Together with the presence of timing noise, this required monitoring close to the epoch of the RXTE observation in order to obtain a good estimate of its period and period derivative. Using a data set that included observations obtained two weeks before and one day after the RXTE observation, we measured a barycentric $P=0.1073889238\,\mathrm{s}$ and $\dot{P}=8.077\times10^{-14}$ for MJD = 53070.210, where the uncertainties are smaller than the precision given here for these quantities.

2.4. Chandra Imaging

Figure 1 shows the ACIS-S3 image of a $20'' \times 20''$ box centered near the position of PSR J1016–5857. As in all Figures, we restrict ourselves to the 0.8–7 keV energy range, since we have found that outside this range there are very few source counts (§ 2.5). In this image we indicate the $1\,\sigma$ error ellipse for the position of the pulsar determined from radio timing measurements (§ 2.3).

We have checked the *Chandra* astrometry by comparing the positions of three X-ray point sources with those of their optical counterparts. In all cases there is an excellent match between positions. In particular, the optical counterpart of CXOU J101623.6-585542, the brightest X-ray point source in the S3 chip (with 300 photons, a hard absorbed spectrum, and flicker-like variability within the 5 hr observation), was selected by positional coincidence from the digitized UK Schmidt plates and the 2MASS survey, at coordinates (2MASS, J2000.0) R.A. = $10^{h}16^{m}23.66$, Decl. = $-58^{\circ}55'42''7$. Its magnitudes from the USNO B1.0 and 2MASS catalogs are B = 15.33, R = 14.35, I =13.94, J = 12.95, H = 12.51, K = 12.35. Figure 2, from the digitized R plate, is a finding chart for this star as well as for the location of the pulsar. A low-resolution ($\sim 15 \,\text{Å}$) spectrum of the star was obtained on 2004 June 23 using the RC Spectrograph and Loral 1K CCD on the SMARTS⁴ 1.5 m telescope at the Cerro Tololo Interamerican Observatory. Three 10 minute exposures were averaged into the raw counts spectrum shown in Figure 3. Emission lines of hydrogen and helium identify this star as an accreting binary, probably a cataclysmic variable, although possibly a low-mass X-ray binary in quiescence. The fact that He II $\lambda 4686$ is stronger than H β indicates high excitation due to X-ray photoionization. The agreement between the X-ray and optical positions of this bright source indicates that the accuracy of the Chandra aspect solution is better than 0".2 in each coordinate and requires no further refinement.

In Figure 1 we see that the centroid of relatively bright X-ray emission is not consistent with the nominal pulsar position. However, considering the systematics involved in obtaining this position, and at the $3\,\sigma$ level (§ 2.3), the position of PSR J1016–5857 coincides with significant X-ray emission, and is even marginally consistent with the position of the brightest X-ray pixel (with 14 photons), at

(J2000.0) R.A. = $10^{h}16^{m}21.35$, Decl. = $-58^{\circ}57'11.3$.

Figure 4 shows the radial profile of counts extracted from a circular region 30" in radius centered within one pixel of the brightest X-ray pixel in Figure 1. We compared the radial profile to that expected from a point source as determined by a ChaRT + MARX raytrace simulation of the PSF at the appropriate position on the focal plane⁵. The centrally peaked region of emission is found to be inconsistent with a point source, but rather shows some extended emission within 2'' of the central pixel. This does not necessarily imply that the pulsar is surrounded by an extended structure $\hat{1}'' - 2''$ in size of approximate circular symmetry, since we do not know the exact pulsar position. In fact we cannot obviously decompose this centrally peaked emission into a clear point source superimposed on a smooth background, and it is possible that the pulsar is a faint source not resolved against the nebular background.

In Figure 5 we show the exposure-corrected image of the full S3 chip, with smoothing on two different scales (in the same Figure we also display radio data from the MOST MGPS2 survey⁶, that we discuss in § 3). While X-ray emission drops off rather abruptly to the SW of the pulsar position, there is a faint "tongue" of emission about $1' \times 2'$ in size toward the NE. This is quantified in Figure 6, where we use the standard-processed event files to extract counts from a rectangular region covering approximately the tongue, but excluding the bright point source CXOU J101623.6-585542 to the north of the pulsar, and including a substantial area to its SW. Here we see that X-ray emission is brightest in an area of half-width $\approx 25''$ (that is approximately circular in shape; cf. Fig. 5), within which it is centrally peaked (see also Fig. 4). Also, X-ray emission drops abruptly to the SW of the pulsar position (negative offsets in the Figure), to a level that we define as a baseline here, but it remains substantially above this background toward the NE, for at least 2'. Beyond this offset, mirror vignetting (not corrected for) becomes significant. In any case, it is clear from the asymmetry in the profile shown that the tongue noted in the smoothed Figure 5 is a real feature.

2.5. Chandra Spectroscopy

As seen in Figure 6, the majority of the counts near the pulsar position lie within a region of $\sim 50''$ in extent, that has approximate circular symmetry (see also Fig. 5). In order to obtain a spectrum of this "core" region, we extracted counts from a circular aperture of radius 50 pixels (r=25'') centered around the pixel with the most photons. For the background we used an annulus with the same center, and inner and outer radii of 55 and 150 pixels, respectively. Virtually all of the photons in the source region are in the 0.8–7.0 keV range, which we used for spectral fits. In this energy range there are 367 background-subtracted counts within the r=25'' aperture.

We extracted a spectrum by grouping the 367 counts with at least 30 counts per bin. We then used the SHERPA spectral fitting package to obtain model parameters. The spectrum is well fitted ($\chi^2_{\nu}=0.97$) by a power-law model with photon index $\Gamma=1.32\pm0.25$, absorbing neutral hydrogen column density $N_{\rm H}=(0.50\pm0.000)$

 $^{^4}$ Small and Moderate Aperture Research Telescope System; see http://www.astro.yale.edu/smarts.

⁵ Following the method outlined in http://cxc.harvard.edu/chart.

⁶ See http://www.physics.usyd.edu.au/astrop/most/mgps.html.

 $0.17) \times 10^{22} \, \mathrm{cm^{-2}}$, and unabsorbed flux $F(0.8-7 \, \mathrm{keV}) = 2.8 \times 10^{-13} \, \mathrm{ergs \, cm^{-2} \, s^{-1}}$, where uncertainties are given at the 68% confidence level. Other models (such as blackbody) give fits that are either unphysical (e.g., with an extremely high temperature of $\sim 1 \, \mathrm{keV}$ and essentially zero N_{H}) or statistically inadequate.

We also extracted counts from a circle with only 10% the area of the above extraction region, with r=15 pixels (cf. Fig. 1). There are 225 background-subtracted counts in this region, and the best power-law fit has the same Γ and $N_{\rm H}$ as the one made to the larger area, although because of inadequate statistics the formal fit is poor.

Finally, we placed an upper limit on emission from the pulsar itself. We did this by extracting counts from a circle three pixels in radius centered at various locations near the peak of emission (see Figs. 1 and 4) and finding which circle contained the greatest flux. This leads to a very conservative limit, both because we have no indication that this corresponds to the actual pulsar position, and also because it assumes no superimposed nebular emission at the pulsar location, which is unreasonable. The 114 photons extracted from this small circular region correspond, assuming the same spectral parameters as above (absorbed power law with $\Gamma=1.32$ and $N_{\rm H}=5\times10^{21}\,{\rm cm}^{-2})$, to an unabsorbed pulsar flux $F(0.8-7\,{\rm keV})<9\times10^{-14}\,{\rm ergs\,cm}^{-2}\,{\rm s}^{-1}$.

The tongue of emission toward the NE of the pulsar position (cf. Figs. 5 and 6) is too diffuse and faint for a useful spectral fit to be made, with only ~ 200 background-subtracted counts (with a very large uncertainty) in an area $\sim 2 \, \mathrm{arcmin}^2$.

2.6. RXTE Search for Pulsations

The data were processed using the recommended methods and with the photon arrival times corrected to the solar system barycenter using the JPL DE200 ephemeris (Standish 1990) for the radio source position (§ 2.3). Selecting good data time intervals using the standard criteria produced a total of 55.5 ks of usable data. In our PCA timing analysis we selected events from PI channels 2–50 (\sim 2–21 keV) and PCA layer 1 only, optimal for a typical pulsar search, obtaining a total of 1.27×10^6 events.

Event times were folded into 20 phase bins at and around the pulsar period determined from the radio ephemeris (§ 2.3), and tested against a flat distribution using a χ^2 statistic. No significant signal was found in a 1024 bin periodogram within $\pm 2.4\,\mu\mathrm{s}$ of the expected period.

3. DISCUSSION

Camilo et al. (2001) argued that PSR J1016–5857 is located near an *Einstein* X-ray source that could be a PWN. Also, based on the location of the pulsar at the tip of a finger of radio emission apparently joined to the SNR G284.3–1.8 (see Fig. 5), they speculated that the two objects might be associated. In that case, the pulsar would be located at the SNR distance, $d=3\pm0.6\,\mathrm{kpc}$ (Ruiz & May 1986). The dispersion measure of the pulsar, DM = 394 cm⁻³ pc (Camilo et al. 2001), and models for the free electron density, suggest a much larger distance $d=9^{+3}_{-2}\,\mathrm{kpc}$ (Taylor & Cordes 1993) or $d\approx8\,\mathrm{kpc}$ (Cordes & Lazio 2002), although these models can be in error for

individual objects by factors of a few.

The Chandra observation of PSR J1016–5857 shows that the pulsar is positionally coincident with a centrally peaked compact X-ray source (§ 2.4) whose spectrum is well modeled by an absorbed power law with photon index $\Gamma = 1.3 \pm 0.3$ (§ 2.5). Both of these characteristics confirm that PSR J1016-5857 is associated with a newly identified PWN that we designate G284.0-1.8 based on its coordinates. Whether or not the pulsar is exactly coincident with the peak of X-ray emission (see Fig. 1 and § 2.4) does not alter this conclusion (see, e.g., Gaensler et al. 2001). Likewise, while the non-thermal compact source has a harder spectrum than many PWNe (e.g., Gotthelf 2003), other well-established PWNe (e.g., Halpern et al. 2002) have photon indices that are consistent, within the uncertainties, with those of G284.0-1.8. PSR J1016-5857/PWN G284.0-1.8 joins about 13 Vela-like pulsars now detected at X-ray energies (see Gaensler et al. 2003; Possenti et al. 2002, and references therein).

The apparent X-ray source identified in *Einstein* data (where a 3' extraction radius was used; Camilo et al. 2001), was about 3 times brighter than what we infer for PWN G284.0–1.8 (including the faint diffuse emission). Part of this discrepancy arises from the inclusion of the bright point source CXOU J101623.6–585542 (Fig. 5) in the *Einstein* extraction region, but after accounting for this a factor of ~ 2 remains unexplained. This point source is likely an accreting binary (see § 2.4), unrelated to the PWN, and is variable within the *Chandra* observation, providing a possible explanation for the remaining discrepancy.

The neutral hydrogen column density obtained from the spectral fits (§ 2.5), $N_{\rm H}=(0.50\pm0.17)\times10^{22}\,{\rm cm}^{-2}$, is one-third of the total Galactic value in this direction estimated from the HI study of Dickey & Lockman (1990), $N_{\rm H}\approx1.50\times10^{22}\,{\rm cm}^{-2}$. This argues that PSR J1016–5857 is located substantially nearer than the DM-derived $d\sim9\,{\rm kpc}$: at Galactic latitude $b=-1^\circ.88$, the height above the plane would be 300 pc, essentially above the Galactic dust layer, leading one to expect the maximum neutral column density. While the conversion of column density to distance is crude, and our $N_{\rm H}$ value has a significant uncertainty, the X-ray data are consistent with $d\sim3\,{\rm kpc}$, and hereafter we parametrize distance by $d_3=d/(3\,{\rm kpc})$.

In § 2.5 we obtained X-ray fluxes in the energy range of the detected photons, 0.8–7 keV. Hereafter we quote spectral quantities in the 2–10 keV range. The isotropic X-ray luminosities obtained from our data are $L_{\rm X\,pwn}=3\times10^{32}\,d_3^2\,{\rm ergs\,s^{-1}}$, and $L_{\rm X\,psr}<9\times10^{31}\,d_3^2\,{\rm ergs\,s^{-1}}$. In terms of the pulsar spin-down luminosity, these luminosities are $L_{\rm X\,pwn}/\dot{E}=1.1\times10^{-4}\,d_3^2$ and $L_{\rm X\,psr}/\dot{E}<3.5\times10^{-5}\,d_3^2$. This efficiency and upper limit for conversion of rotational kinetic energy to X-rays are lower than for many PWNe/pulsars (e.g., Possenti et al. 2002), but are similar to those of Vela (Helfand et al. 2001; Pavlov et al. 2001) and other Vela-like objects (e.g., Halpern et al. 2001). The non-detection of pulsations from PSR J1016–5857 in the RXTE observation (§ 2.6) is consistent with this upper limit on unpulsed emission: assuming a best-case scenario with pulsed fraction of 100% and duty cycle of 5%, we would have expected an RXTE signal-to-noise ratio $\lesssim 6$.

The EGRET source 3EG J1013-5915 has a photon index $\Gamma = 2.32 \pm 0.13$ (Hartman et al. 1999) that is consistent with those of some Vela-like pulsars (e.g., Halpern et al. 2001), apparently has a steady flux (McLaughlin et al. 1996), as is the case for other pulsar-powered γ ray sources, and its isotropic luminosity above 100 MeV is $L_{\gamma}/E = 0.06 d_3^2$ (Camilo et al. 2001). Using the Chandra observation, $L_{\gamma}/L_{X} \sim 500$, and PSR J1016-5857 remains a viable candidate for generating the γ -rays detected from 3EG J1013-5915. Pulsars are the only established class of Galactic objects that power EGRET sources, but CXOU J101623.6–585542 (see \S 2.4), a relatively bright and hard X-ray source whose exact nature is unknown, should probably not be dismissed out of hand as a possible contributor to 3EG J1013-5915. These two are the brightest X-ray sources in the Einstein field of this region (cf. Camilo et al. 2001). However, that observation covered only about 1/3 of the area of the 3EG J1013-5915 error box (the *Chandra* S3 chip covers only 1% of the box, and the roll angle of the observation was such that most other ACIS CCDs did not fall within the EGRET box), and it is possible that another heretofore undetected X-ray source is in fact responsible for 3EG J1013-5915. An incontrovertible conclusion on this matter will likely require the GLAST observatory.

As noted in § 2.4, the brightest component of PWN G284.0-1.8 (Fig. 1), superimposed on fainter emission, is not consistent with a point source (Fig. 4). By analogy with the structures now observed surrounding many young and energetic pulsars (see, e.g., Ng & Romani 2004), we speculate that this structure may indicate the pulsar wind termination shock. If so, $r_s \approx 2'' = 0.03 d_3 \,\mathrm{pc}$, similar in size to that of the Vela pulsar (Helfand et al. 2001). Proceeding further with this interpretation one runs into familiar problems: a simple estimation of the nebular magnetic field downstream of the shock obtained from the assumption of equipartition suggests a few tens of μG , and the corresponding synchrotron lifetime of electrons/positrons at $\sim 1.5 \,\mathrm{keV}$ (the peak of our observed energy distribution) is so short (a few hundred years or less) that the very high velocity required to transport the particles to the edge of the PWN is at variance with more reasonable nebular expansion speeds (e.g., Kennel & Coroniti 1984; van der Swaluw et al. 2001). In any case, despite the limitations of existing X-ray data on PSR J1016–5857/PWN G284.0–1.8 that prevent further quantitative analysis, the system shows several characteristics similar to, or consistent with, those of other Vela-like pulsars/PWNe.

We now discuss the tongue of X-ray emission that has PSR J1016–5857 and its $\sim 25''$ PWN located near its SW end (Figs. 5 and 6), as well as the possible association of the pulsar with SNR G284.3–1.8. While the $\approx 1' \times 2'$ X-ray feature is real (§ 2.4), we have no a priori expectation that it should be associated with the pulsar. The pulsar and this extended feature are both located, in projection, $\sim 4'$ to the west of the bright (in radio) western edge of SNR G284.3–1.8 (see Fig. 5). The SNR in turn is interacting with a molecular cloud (Ruiz & May 1986). It is therefore possible that the very faint and extended X-ray emission is somehow related to the SNR/molecular cloud and not to the pulsar.

On the other hand, as mentioned before, the pulsar is located at the SW tip of a relatively bright finger of radio emission that appears to connect at its NE end to the SNR (Fig. 5; Milne et al. 1989; Camilo et al. 2001). It is notable that the X-ray tongue provides a good match to the SW tip of the radio finger, in both width and position anglewith the pulsar also located very near the SW end of X-ray emission. These coincidences are suggestive of a possible connection between the radio finger and X-ray tongue, and in turn of the pulsar with both of them. The length of the tongue NE of the pulsar is $L \approx 2' = 1.8 d_3$ pc, with a SW extension < 0.2 (Fig. 6). If the X-ray tongue is related to the pulsar, its cause is not clear, since it is not easy to understand how such a large distance could be covered within the short synchrotron lifetimes of the radiating particles. It has been suggested (e.g., Wang et al. 1993) that wind acceleration can occur to generate very large velocities, but this should result in visible collimation, which we do not observe here. Also, in cases where pulsars travel supersonically through the ambient medium, a bow shock develops due to ram pressure with the pulsar at one end of what is often a bright elongated PWN that gradually fades opposite the direction of motion (e.g., Gaensler et al. 2004). However, in the present case the pulsar velocity required would likely be several $1000 \,\mathrm{km \, s^{-1}}$, and in any case the X-ray emission again does not appear to be very collimated as would be expected. If somehow such a large velocity can explain these observations, then the pulsar would presumably be traveling due SW, rather than due west as might be expected if it had originated from the apparent center of SNR G284.3-1.8, a reminder that even if the pulsar is related to the radio finger and X-ray tongue, the connection to the SNR would not necessarily be established, since the objects could appear close merely in projection.

The PSR J1016-5857/PWN G284.0-1.8 system shows significant parallels to PSR B1823-13/PWN G18.0-0.7, another Vela-like pulsar with parameters very similar to those of J1016–5857. A deep XMM observation of B1823-13 (Gaensler et al. 2003) shows that the pulsar and its compact PWN are embedded asymmetrically within a fainter and much larger nebula whose origin is not entirely clear (two potentially important differences between the systems are that no SNR is detected near B1823-13, and also that its inferred wind-termination shock radius is an order of magnitude larger than for J1016–5857). Further observations are required in order to understand fully the structures observed near PSR J1016-5857 and their relationships: radio observations may reveal in detail whether the radio finger is related to the SNR, and whether the finger emission is non-thermal or polarized, and how it evolves along its length toward the pulsar at its end. Xray observations may reveal useful spectral information and show whether the extended emission, if non-thermal, has a softer spectrum than that of the compact PWN near the pulsar position due to synchrotron losses, and help elucidate its origin.

We are grateful to Charles Bailyn for obtaining, using the SMARTS 1.5 m telescope, the optical data described in § 2.4. We thank Vicky Kaspi for early contributions to this work. We are grateful to Marta Burgay and Andy Faulkner for helping with data collection at Parkes. The

Parkes Observatory is part of the Australia Telescope, which is funded by the Commonwealth of Australia for operation as a National Facility managed by CSIRO. We thank Dick Hunstead and Anne Green for supplying the radio image used in Figure 5. The Molonglo Observatory Synthesis Telescope is supported by the Australian Research Council. FC thanks Caleb "Tweety Bird" Scharf for his irrepressible good humor and patience. This work was supported by NASA through SAO grant GO3-4076X.

REFERENCES

Camilo, F., et al. 2001, ApJ, 557, L51 Cordes, J. M., & Lazio, T. J. W. 2002, preprint (astro-ph/0207156) Dickey, J. M., & Lockman, F. J. 1990, ARA&A, 28, 215 Gaensler, B. M., Pivovaroff, M. J., & Garmire, G. P. 2001, ApJ, 556,

Gaensler, B. M., Schulz, N. S., Kaspi, V. M., Pivovaroff, M. J., & Becker, W. E. 2003, ApJ, 588, 441
Gaensler, B. M., van der Swaluw, E., Camilo, F., Kaspi, V. M.,

Baganoff, F. K., Yusef-Zadeh, F., & Manchester, R. N. 2004, ApJ, in press (astro-ph/0312362)

Gotthelf, E. V. 2003, ApJ, 591, 361 Halpern, J. P., Camilo, F., Gotthelf, E. V., Helfand, D. J., Kramer, M., Lyne, A. G., Leighly, K. M., & Eracleous, M. 2001, ApJ, 552,

Halpern, J. P., Gotthelf, E. V., Camilo, F., Collins, B., & Helfand, D. J. 2002, in Neutron Stars in Supernova Remnants, eds. P. O.

Slane & B. M. Gaensler (San Francisco: ASP), 199
Hartman, R. C., et al. 1999, ApJS, 123, 79
Helfand, D. J., Gotthelf, E. V., & Halpern, J. P. 2001, ApJ, 556, 380
Hobbs, G., et al. 2004, MNRAS, in press (astro-ph/0405364)

Jahoda, K., Swank, J. H., Giles, A. B., Stark, M. J., Strohmayer, T., Zhang, W., & Morgan, E. H. 1996, Proc. SPIE, 2808, 59 Kennel, C. F., & Coroniti, F. V. 1984, ApJ, 283, 710 Manchester, R. N., et al. 2001, MNRAS, 328, 17

McLaughlin, M. A., Mattox, J. R., Cordes, J. M., & Thompson,

D. J. 1996, ApJ, 473, 763
Milne, D. K., Caswell, J. L., Kesteven, M. J., Haynes, R. F., & Roger, R. S. 1989, Proc. Astr. Soc. Aust., 8, 187
Ng, C.-Y., & Romani, R. W. 2004, ApJ, 601, 479
Pavlov, G. G., Zavlin, V. E., Sanwal, D., Burwitz, V., & Garmire, G. P. 2001, ApJ, 552, L129
Paccepti, A. Causti, B. Colpi, M. & Marachetti, S. 2002, A&A.

Possenti, A., Cerutti, R., Colpi, M., & Mereghetti, S. 2002, A&A, 387, 993

Ruiz, M. T., & May, J. 1986, ApJ, 309, 667

Standish, E. M. 1990, A&A, 233, 252

Taylor, J. H., & Cordes, J. M. 1993, ApJ, 411, 674 van der Swaluw, E., Achterberg, A., Gallant, Y. A., & Tóth, G. 2001, A&A, 380, 309

Wang, Q. D., Li, Z.-Y., & Begelman, M. C. 1993, Nature, 364, 127

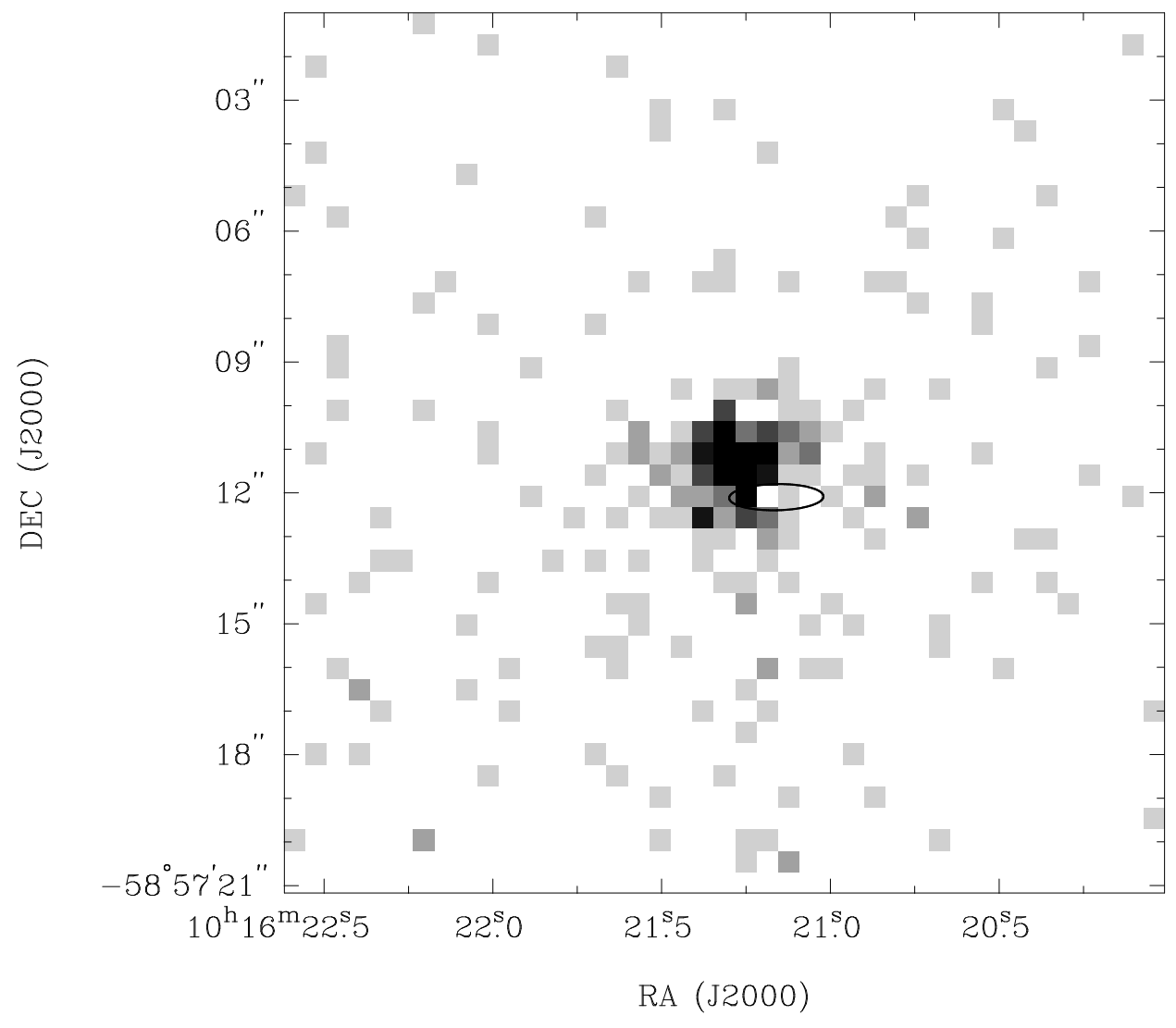


Fig. 1.— Exposure-corrected image in the 0.8–7 keV range with no smoothing, in $20'' \times 20''$ box around PSR J1016–5857. Greyscale is linear, running from 0% to 50% of peak in this field. The ellipse corresponds to the radio pulsar position and $1\,\sigma$ uncertainties obtained from timing measurements (§ 2.3).

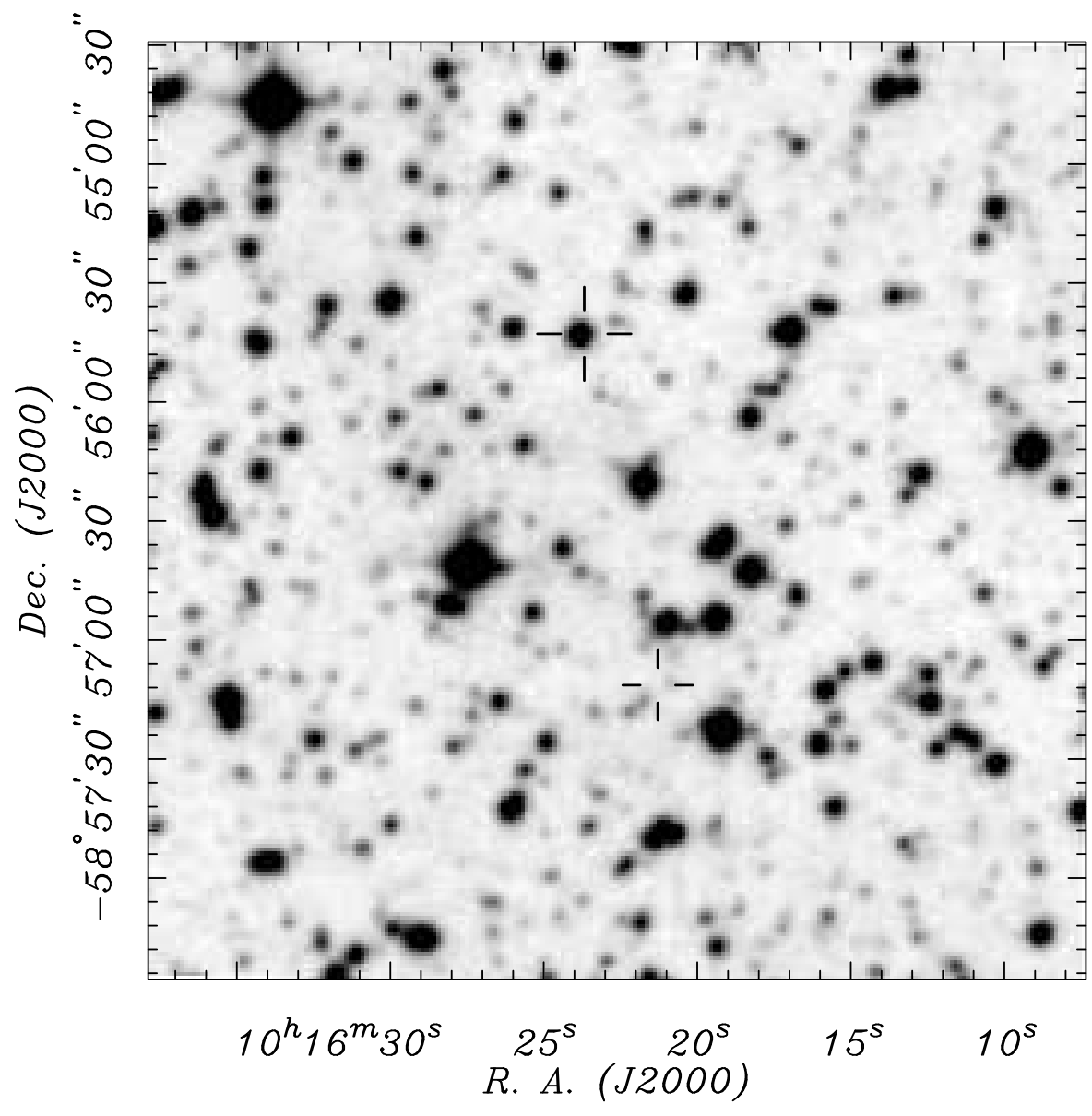


Fig. 2.— A finding chart from a digitized UK Schmidt sky survey red plate showing the locations of PSR J1016–5857 (bottom cross) and the serendipitous X-ray source CXOU J101623.6–585542 (top cross).

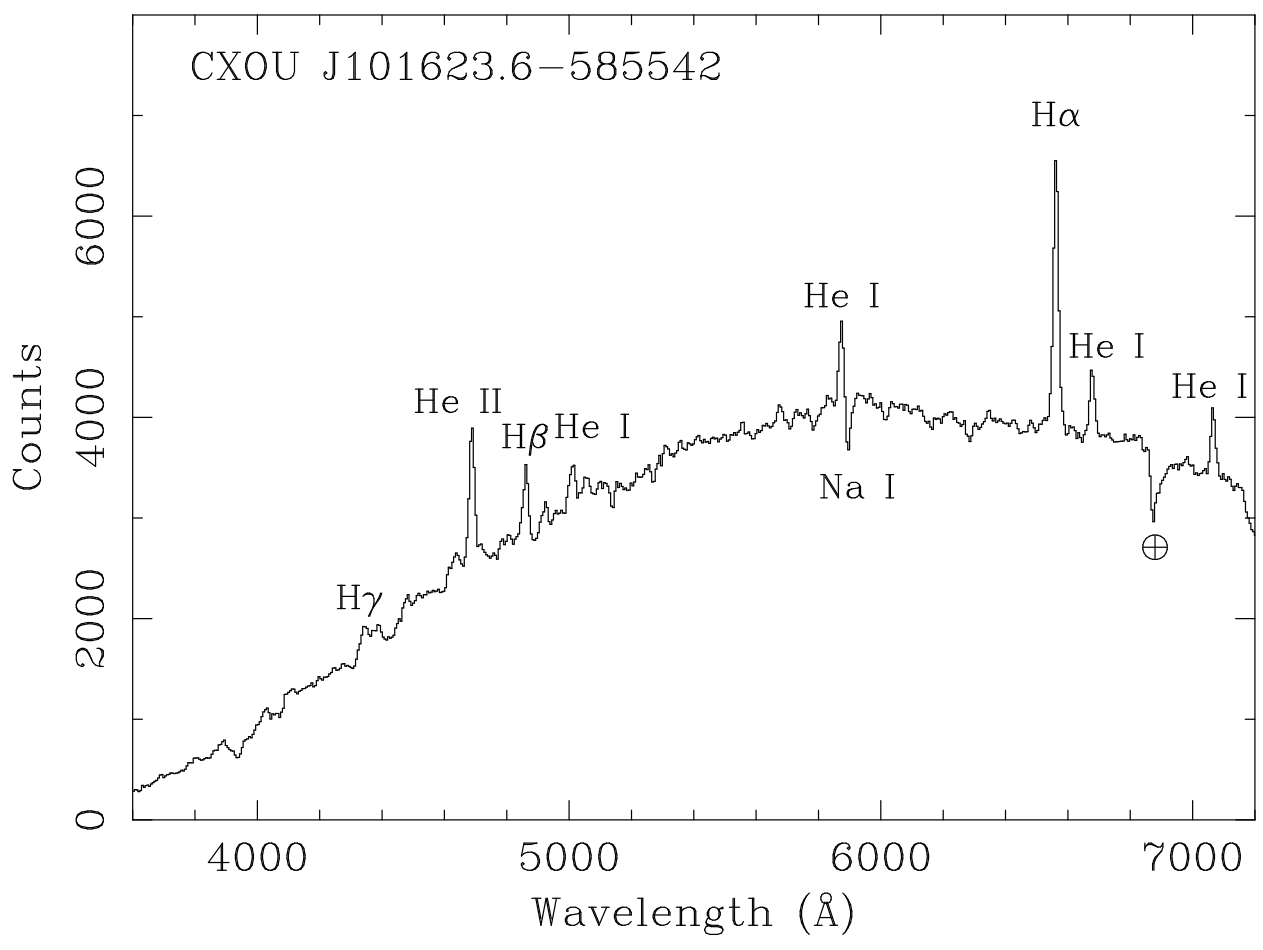


FIG. 3.— A 30 minute exposure spectrum of the optical counterpart of the serendipitous X-ray source CXOU J101623.6–585542 obtained on the SMARTS/CTIO 1.5 m telescope on 2004 June 23 (courtesy C. Bailyn). Flux calibration has not been applied. Prominent emission lines that are typical of accretion-powered binary X-ray sources are marked. There are no obvious stellar photospheric absorption features. Interstellar Na I D absorption is also seen, as well as weaker diffuse interstellar bands. (See Fig. 2 for a finding chart.)

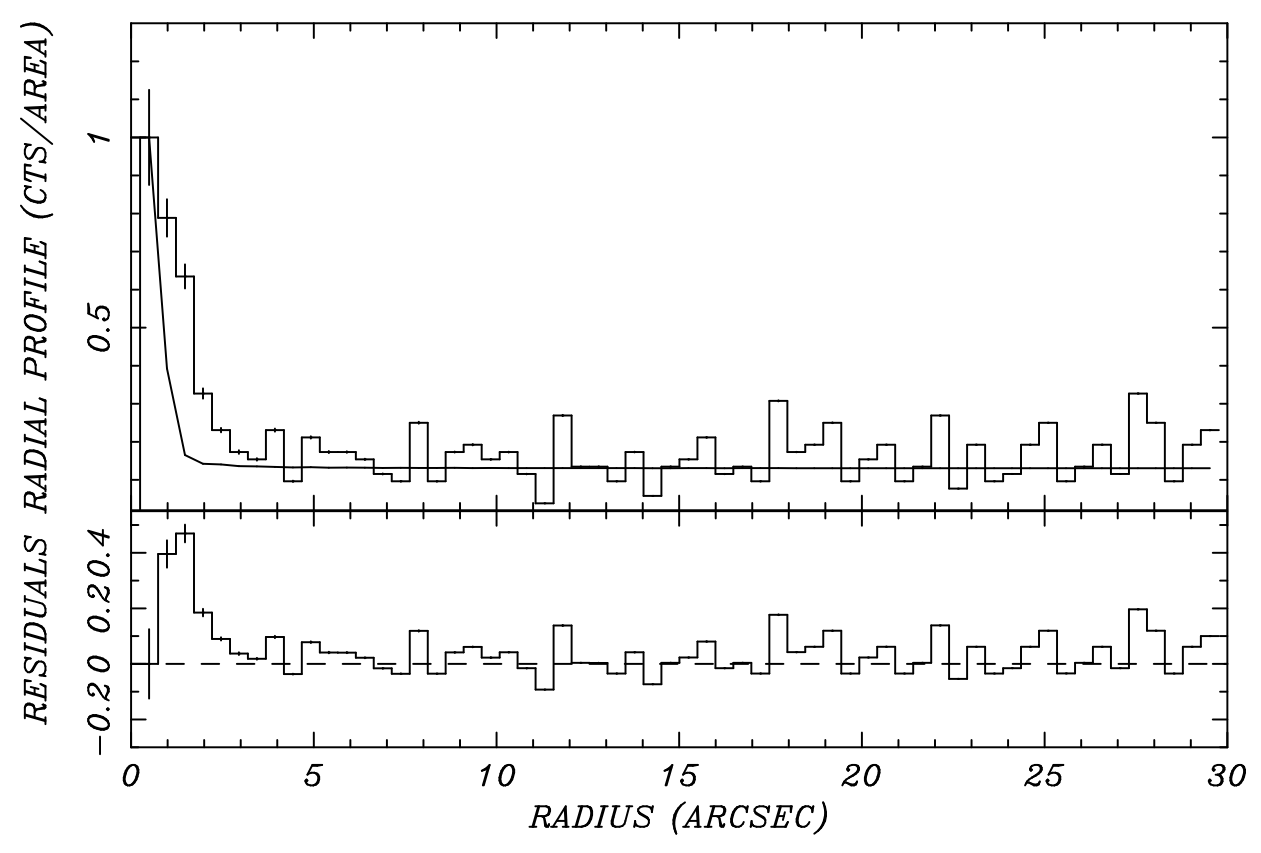


Fig. 4.— Top: Radial profile of 0.8–7 keV counts centered approximately on the peak of emission. The solid line corresponds to the computed PSF, arbitrarily normalized to the central bin. Bottom: Residuals of data minus PSF, showing extended emission within $\sim 2''$ of the center.

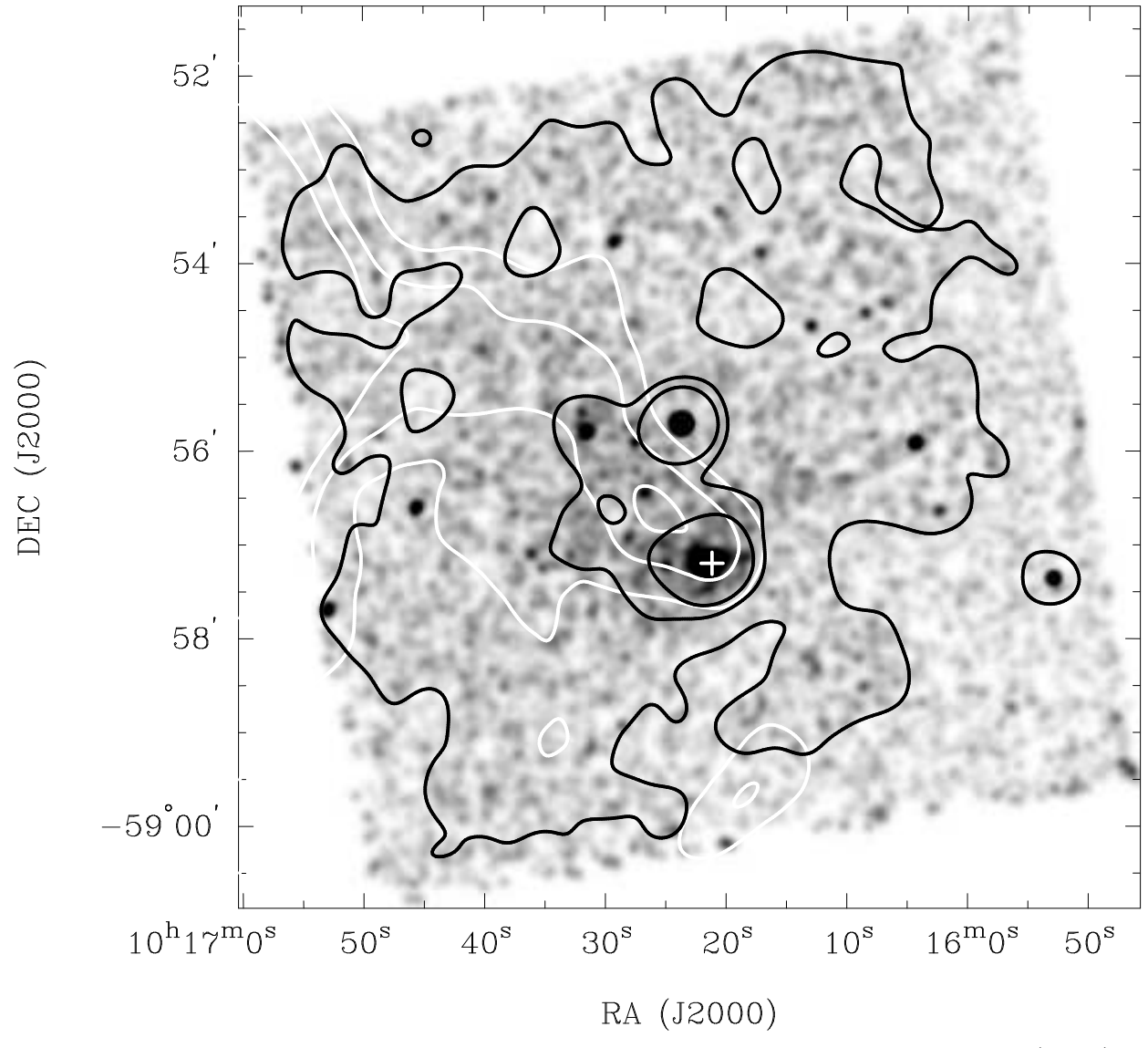


Fig. 5.— Exposure-corrected Chandra image in the 0.8–7 keV range and Molonglo Observatory Synthesis Telescope (MOST) map at a frequency of 843 MHz. Greyscale is X-ray data smoothed with a Gaussian of FWHM = 7", over a linear range of 0% to 4.4% of peak intensity (which occurs in the source CXOU J101623.6–585542 \approx 1.5 to the north of the pulsar). Black contours are the same data smoothed with a FWHM = 30" Gaussian, at levels of 10%, 20%, and 30% of peak. White contours are radio data, at levels of 10, 20, and 30 mJy beam⁻¹, and have a resolution of 43" \times 50". A portion of the western edge of the radio SNR G284.3–1.8 is visible toward the NE corner of the field. The white cross marks the position of PSR J1016–5857.

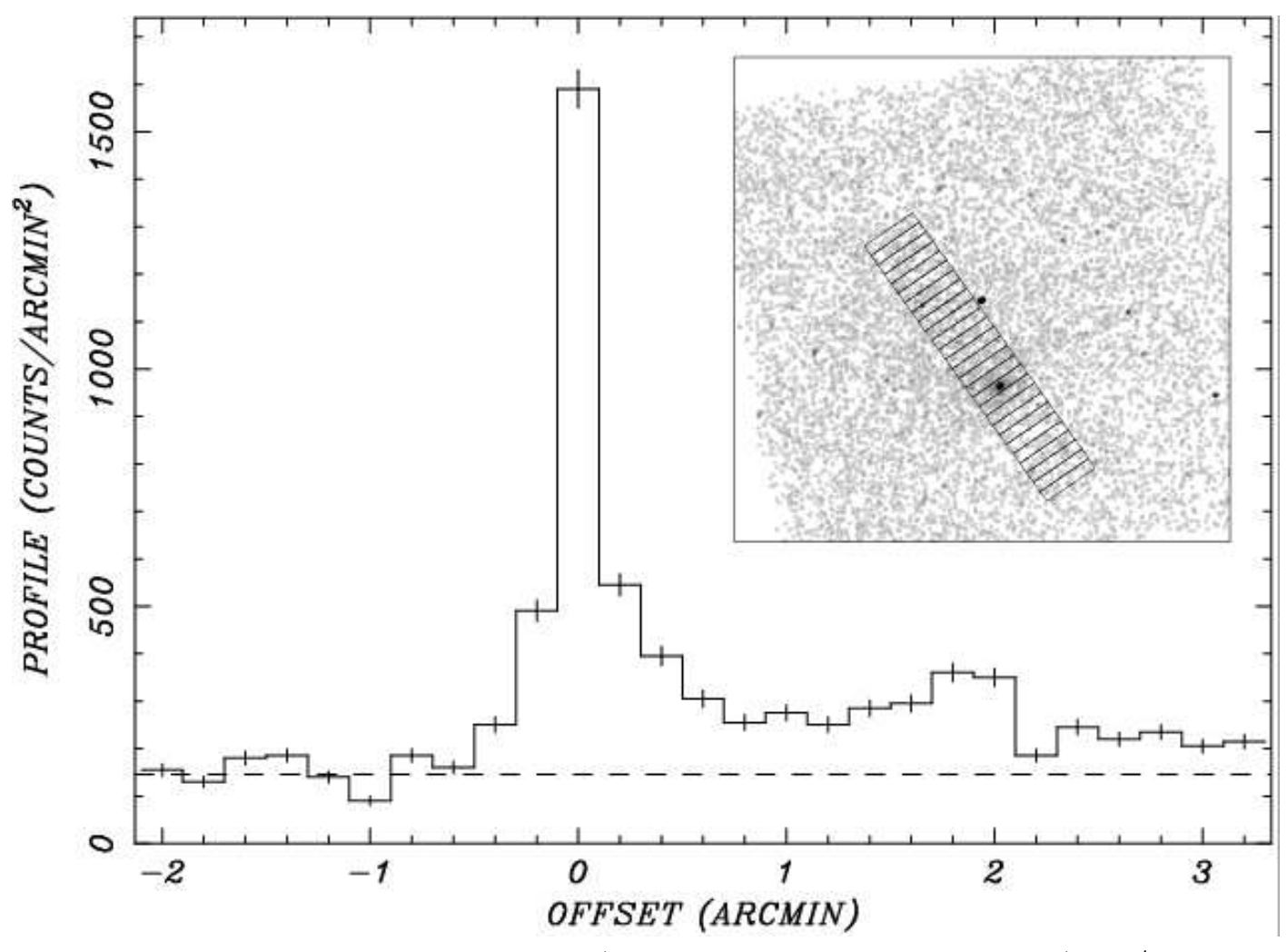


Fig. 6.— Counts extracted from 27 adjacent rectangular boxes (see inset, with north to the top and east to the left), each 1' in width and 0'.2 in length, with the long axis of the overall $1' \times 5'.4$ area oriented at 35° east of north. Zero offset corresponds to the box centered on the position of PSR J1016–5857, with negative offsets in the SW direction and positive offsets in the NE direction. The slight increase in counts seen in the two bins near an offset of 2' is contributed by a point source. Compare to Figure 5.